

# Enhancing Traffic Object Detection in Variable Illumination with RGB-Event Fusion

Zhanwen Liu\*<sup>1</sup>, Nan Yang\*<sup>1</sup>, Yang Wang<sup>†</sup><sup>1</sup>, Yuke Li, Xiangmo Zhao, Fei-Yue Wang

**Abstract**—Traffic object detection under variable illumination is challenging due to the information loss caused by the limited dynamic range of conventional frame-based cameras. To address this issue, we introduce bio-inspired event cameras and propose a novel Structure-aware Fusion Network (SFNet) that extracts sharp and complete object structures from the event stream to compensate for the lost information in images through cross-modality fusion, enabling the network to obtain illumination-robust representations for traffic object detection. Specifically, to mitigate the sparsity or blurriness issues arising from diverse motion states of traffic objects in fixed-interval event sampling methods, we propose the Reliable Structure Generation Network (RSGNet) to generate Speed Invariant Frames (SIF), ensuring the integrity and sharpness of object structures. Next, we design a novel Adaptive Feature Complement Module (AFCM) which guides the adaptive fusion of two modality features to compensate for the information loss in the images by perceiving the global lightness distribution of the images, thereby generating illumination-robust representations. Finally, considering the lack of large-scale and high-quality annotations in the existing event-based object detection datasets, we build a DSEC-Det dataset, which consists of 53 sequences with 63,931 images and more than 208,000 labels for 8 classes. Extensive experimental results demonstrate that our proposed SFNet can overcome the perceptual boundaries of conventional cameras and outperform the frame-based method by 8.0% in mAP50 and 5.9% in mAP50:95. Our code and dataset will be available at <https://github.com/YN-Yang/SFNet>.

**Index Terms**—Traffic object detection, variable illumination, cross-modality fusion, automatic driving.

## I. INTRODUCTION

**T**RAFFIC object detection aims to accurately recognize and locate traffic objects, making it a critical component of autonomous driving systems and serving as the foundation for downstream tasks such as object tracking and trajectory prediction [1]–[4]. Notably, the success of existing traffic object detection methods is heavily contingent upon image quality. However, the limited capacitance capacity in the integral imaging circuit of frame-based cameras restricts their dynamic range [5], making it difficult to achieve stable imaging in poor lighting conditions (e.g., low-light and overexposure), which will result in decreased image contrast and information loss

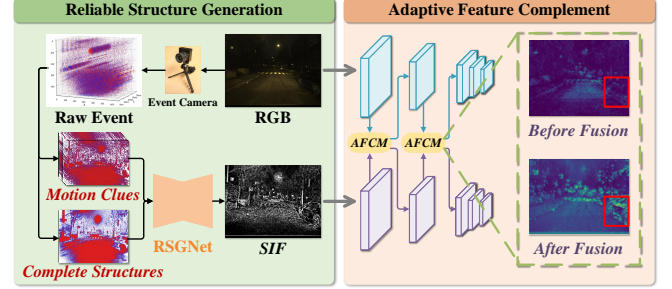


Fig. 1. Our SFNet comprises two key steps: reliable structure generation and adaptive feature complement. Left: Given an RGB image and corresponding event stream, high-quality structural information is generated from the event stream. Right: The event feature is adaptively extracted to compensate for information loss in the image modality. The image feature, before complementation, lacks discriminative characteristics due to information loss and contrast reduction across the image. Notable, after the complementation, the feature becomes more discriminative.

and hinder the extraction of representative features for traffic object detection.

To compensate for the limitations of frame-based cameras, we propose to introduce the bio-inspired event cameras [5]–[12] for traffic object detection. Unlike frame-based cameras, event cameras detect changes in light intensity at the pixel level and asynchronously output the event stream. With high dynamic range (>120 dB), event cameras exhibit remarkable stability and robustness in poor lighting conditions, presenting great potential in traffic object detection under variable illumination conditions. However, the event stream captured by event cameras lacks color and fine-grained texture information, resulting in insufficient semantic information for object detection [13]. To achieve robust traffic object detection under poor lighting conditions, we propose leveraging the complementary properties of both modalities, *i.e.*, the events and images.

To achieve this goal, two challenges must be comprehensively considered and addressed. The first challenge is to overcome the modality differences between events and images and extract high-quality structural information for diverse motion states from the event stream. To this end, a typical solution for existing methods [14]–[21] resort to using a fixed time window to sample and compress temporal information of the event stream, generating image-like tensors for subsequent feature extraction. However, the fixed event sampling is susceptible to introducing sparsity or blurriness issues for moving objects. As shown in Fig. 2(b, c), when the time window is small, slow-moving objects will exhibit sparse structures that can be easily confused with noise [22]; when the time window is large, fast-moving objects will show

\*Co-first author. <sup>†</sup>Corresponding author.

Zhanwen Liu, Nan Yang, Yang Wang and Xiangmo Zhao are with the School of Information Engineering, Chang’an University, Shaanxi, Xi’an 710000, China (e-mail: zwliu@chd.edu.cn; 2022024001@chd.edu.cn; xmzhao@chd.edu.cn).

Yuke Li is with the Waytous Co. Ltd., Beijing 100083, China (e-mail: liyuke14@mails.ucas.ac.cn).

Fei-Yue Wang is with the Institute of Automation, Chinese Academy of Sciences, Beijing 100083, China (e-mail: feiyue.wang@ia.ac.cn).

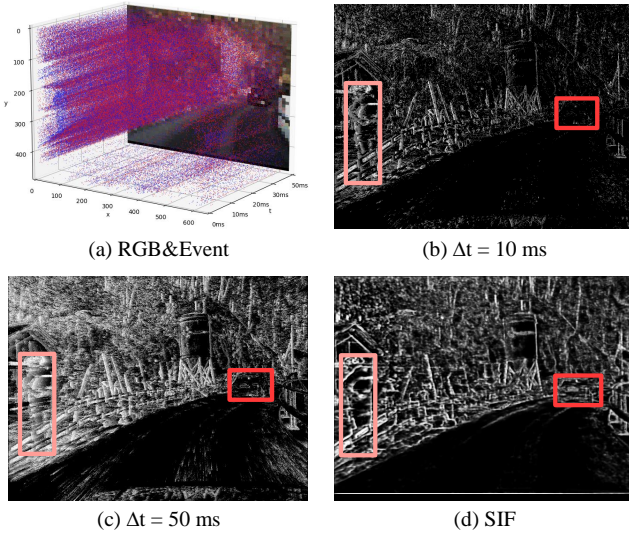


Fig. 2. Fixed time windows for event representation. The pedestrian exhibits fast movement relative to the camera, while the car moves slower. (b) displays a short time window of  $\Delta t = 10\text{ ms}$ , resulting in sparse structures for the car. Conversely, (c) shows a long time window of  $\Delta t = 50\text{ ms}$ , resulting in blurry structures for the pedestrian. Notably, our Speed Invariant Frame in (d) shows the complete structures and sharp edges. We utilize red and pink boxes to mark the car and pedestrian, respectively.

blurry structures that inhibit the structure perceiving [23]. Such low-quality structural information introduces uncertainties in generated features. Therefore, a motion-robust representation method is required to ensure that objects with varying motion speeds can obtain complete and sharp structural information. Further, the poor light conditions will result in non-uniform information loss and contrast degradation across the image. Therefore, another challenge lies in effectively perceiving the degree of information loss and contrast reduction across the image and executing adaptive information compensation. Currently, various fusion methods have been proposed for object detection, which can be categorized into two strategies: late fusion and middle fusion. Late fusion methods [24]–[26] directly combine the detection results of two modalities, but lack interaction between different modalities. Middle fusion methods [27]–[30] achieve fusion by simple concatenation and attention mechanisms during the feature extraction stage. However, these methods cannot effectively perceive the degrees of information loss across the images and fail to adaptively complement information, which is essential for object detection in variable illumination conditions.

To address the above issues, we propose a novel Structure-aware Fusion Network (SFNet), which consists of two key components: Reliable Structure Generation Network (RSGNet) and Adaptive Feature Complement Module (AFCM), accounting for motion-robust high-quality structural information generation and illumination-robust representations modeling through adaptive cross-modality fusion, respectively, as shown in Fig. 1. Specifically, first, the RSGNet is devised to generate Speed Invariant Frames (SIF) by using a large time window to aggregate complete structural information for slow-moving objects and generating sharp edges for fast-moving

objects with the assistance of motion cues extracted from event stream, capable of handling diverse motion states. The resulting SIF is motion-robust and provides complementary structural cues for images. Second, the AFCM is designed to perceive the lightness distribution in images by calculating the global spatial correlation between image and event modalities, which is used to guide the adaptive feature fusion between image and event modalities. Besides, considering the impact of noise in the event stream on the fusion process, we leverage the local smoothness of the image modality to suppress event noise. This adaptive fusion process allows us to leverage the strengths of both modalities and tailor the feature fusion to information loss of each region in images. Finally, to facilitate further research on RGB-Event fusion-based object detection, we provide rich and accurate object detection annotations on the DSEC dataset [31] and propose the DSEC-Det dataset.

In summary, the main contributions of this paper are as follows:

- (1) We propose a RSGNet, which generates Speed Invariant Frames to ensure the integrity and sharpness of structures for objects with diverse motion states.
- (2) We design an AFCM, which estimates information loss by perceiving the lightness distribution of the image modality and adaptively extracts event features to complement it.
- (3) We build a large-scale RGB-Event object detection dataset DSEC-Det, comprising accurate object detection annotations and diverse driving scenes with variable illumination conditions.
- (4) We benchmark various state-of-the-art object detection methods on our dataset and demonstrate that our SFNet significantly outperforms existing methods.

## II. RELATED WORK

This section first provides a comprehensive overview of the event-based object detection datasets. Subsequently, we review existing event-based object detection methods and event representation methods.

### A. Datasets

**Event modality.** The datasets in the event modality include the Gen1 dataset [32] and the 1 Mpx dataset [13], both of which contain substantial data. Gen1 includes over 255,000 labeled cars and pedestrians with a resolution of  $304 \times 240$  and annotated frequencies of 1 Hz, 2 Hz, or 4 Hz. 1 Mpx includes over 25 million labeled pedestrians, two wheelers, cars, trucks, buses, traffic signs, and traffic lights with a higher resolution of  $1280 \times 720$  and an annotated frequency of 60 Hz. However, both datasets exclusively contain event modality data and not publicly released image modality data.

**RGB&Event modality.** EventKITTI [33] utilizes the ESIM [34] simulator to generate event data for the KITTI [35] dataset, yet the simulated events significantly differ from real events. Some works [29] [30] partition subsets of the DSEC dataset [31] for building object detection datasets. Tomy *et al.* [29] annotates the training set of the DSEC dataset with three classes. However, this dataset contains considerable noise in the labels. Zhou *et al.* [30] selects 16 sequences from the

DSEC dataset to annotate bounding boxes for traffic motion objects. However, they annotate only 13,314 images without specifying object classes. Hence, a large-scale and high-quality RGB-Event traffic object detection dataset is still scarce. To address this problem, we manually annotate all sequences of the DSEC dataset and propose the DSEC-Det dataset, which has a larger scale, richer object classes, and higher annotation quality compared to the aforementioned dataset.

### B. Event-Based Object Detection

**Event-based detection methods.** Benefiting from the outstanding attributes of event cameras, numerous event-based detection methods have been proposed, including RED [13], ASTMNet [36] and RVT [37]. RED [13] proposes a recurrent network architecture that uses ConvLSTM to extract spatiotemporal features from the event stream. ASTMNet [36] proposes a temporal attention convolutional module to learn event feature embedding from continuous event streams and a lightweight spatiotemporal memory module to extract temporal clues. RVT [37] proposes a novel backbone for object detection that can reduce the inference time significantly while retaining similar performance to prior works. However, the lack of color and fine-grained texture information in event streams results in insufficient semantic information, which is important to the detection task.

**RGB and event fusion-based detection methods.** Detection by combining RGB and event streams is a reliable way to achieve high-performance object detection, which can be categorized into two strategies: late fusion and middle fusion. Late fusion methods include [24]–[26]. Chen *et al.* [24] uses non maximum suppression (NMS) to fuse the detection results of two modalities. Li *et al.* [26] utilizes the Dempster-Shafer theory to fuse the detection results of the two modalities. While Jiang *et al.* [25] proposes to fuse confidence maps of the two modalities. However, these late fusion methods lack intermodal interactions and fail to leverage the complementary nature effectively. Then, several middle fusion methods [27]–[30] are proposed to guide the fusion of two modalities on the feature level. Liu *et al.* [27] computes a channel attention map to guide the learning of image features based on event features. Cao *et al.* [28] generates pixel-level attention maps based on features from two modalities and multiplies them with image features to obtain the fused features. Tomy *et al.* [29] uses a simple concatenation operation to combine features from two modalities at different resolutions. Zhou *et al.* [30] proposes a bidirectional fusion module to model multimodality features in the spatial and channel dimensions to form a shared representation. However, these methods cannot effectively perceive the information loss occurring in the images and adaptively compensate for it. To address this issue, we propose AFCM that perceives the global lightness distribution in images by calculating the global spatial correlation between the image and event modalities, and guides the interaction of the two modalities, allowing for a more comprehensive fusion of their respective strengths.

### C. Event Representation

Since events are sparse impulse signals that cannot be directly processed using DNN methods, some scholars propose to convert the events into synchronous image-like tensors for processing. These methods can be roughly divided into image-based [14]–[16], surface-based [17]–[19], and voxel-based [20] [21] methods and are widely applied to computer vision tasks such as image classification, action recognition, and object detection [38].

The image-based methods include Event Histogram [14], Event Image [15] and Timestamp [16]. While image-based approaches are straightforward to process, they tend to lose substantial temporal information. Surface-based methods, such as Time Surface [17], HATS [18], and DiST [19], normalize timestamps to preserve temporal information of the event stream. Voxel-based methods, such as Voxel Grid [20] [21], map original events to different time grids based on interpolation methods, to further preserve time dimension information. Nevertheless, they commonly opt for fixed time windows tailored to particular tasks and scenes, leading to low-quality structural information extraction during slow and fast-motion scenarios. To tackle this issue, we propose a Reliable Structure Generation Network (RSGNet) that obtains Speed Invariant Frames (SIF) which are robust to diverse motion states by effectively combining structural information and motion cues extracted from large range events.

## III. PROPOSED METHODS

This section first introduces the event imaging mechanism and output format in Section III-A. Next, Section III-B describes the overall architecture of the proposed method. Section III-C introduces the details of the Reliable Structure Generation Network (RSGNet), uncovering its inner workings. Finally, Section III-D presents the design of the Adaptive Feature Complement Module (AFCM), shedding light on its purpose and functionality.

### A. Event Camera Introduction

The event camera outputs an event  $(x_i, y_i, p_i, t_i)$  when the light intensity  $\mathcal{L}$  changes at a pixel and exceeds the contrast threshold  $c$ .  $(x_i, y_i)$  represents the spatial coordinates of pixel  $i$ ,  $t_i$  represents the timestamp when the event is triggered, and  $p_i \in \{-1, 1\}$  indicates the event polarity. The values 1 and -1 represent the increasing or decreasing change in intensity at the pixel, respectively. This process can be formulated as follows:

$$p_i = \begin{cases} +1, & \text{if } \log \left( \frac{\mathcal{L}_t(x_i, y_i)}{\mathcal{L}_{t-\Delta t}(x_i, y_i)} \right) > c, \\ -1, & \text{if } \log \left( \frac{\mathcal{L}_t(x_i, y_i)}{\mathcal{L}_{t-\Delta t}(x_i, y_i)} \right) < -c, \end{cases} \quad (1)$$

where  $\mathcal{L}_t(x_i, y_i)$  and  $\mathcal{L}_{t-\Delta t}(x_i, y_i)$  represent the intensity at  $t$  and  $t - \Delta t$ , respectively.

### B. The Overview of the SFNet

In this section, we show the details of the Structure-aware Fusion Network (SFNet), which utilizes RGB and event



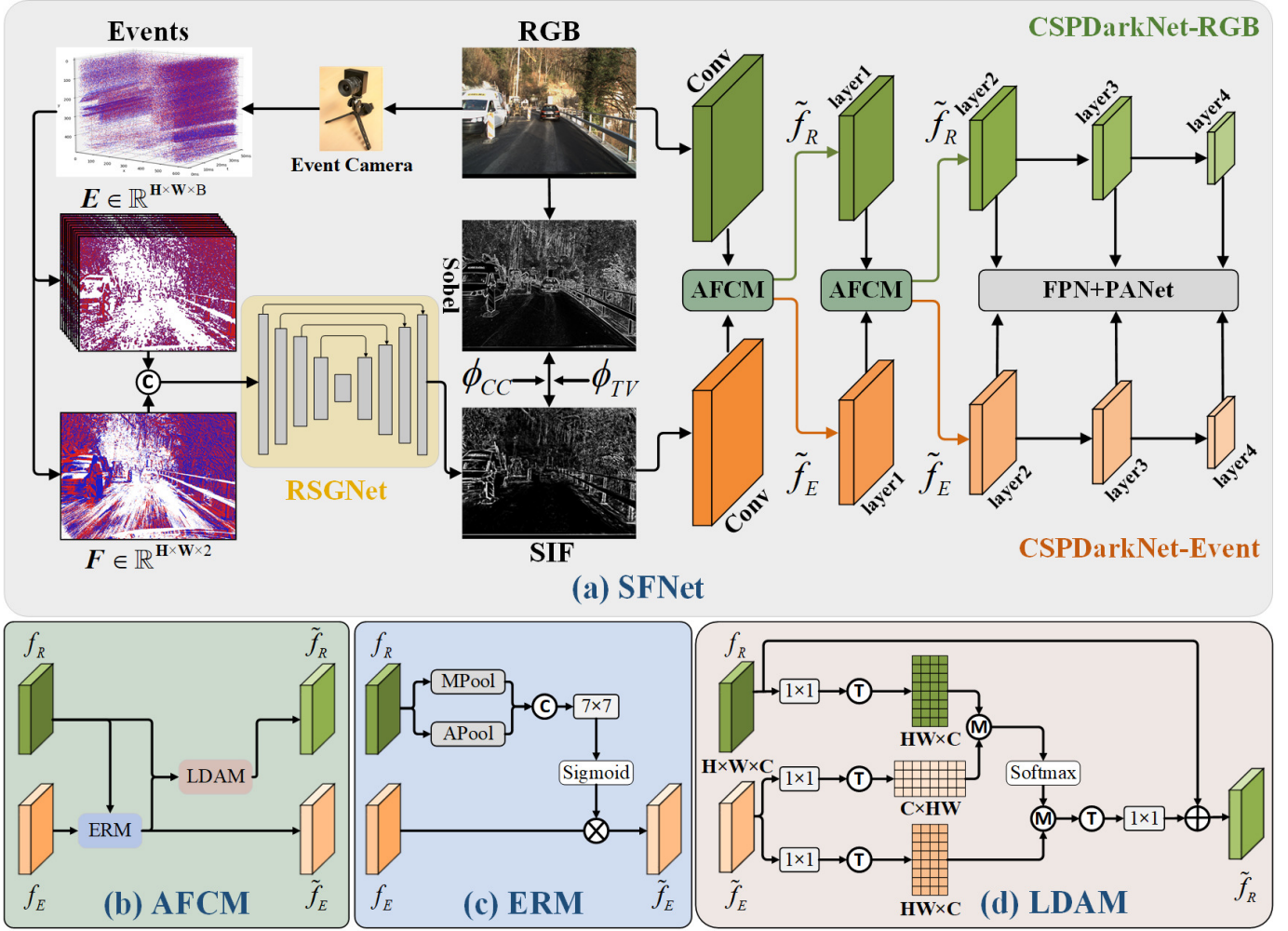


Fig. 3. The pipeline of the proposed Structure-aware Fusion Network (SFNet). The event frame  $F$  and event polarity integration  $E$  generated from the event stream are concatenated and fed into the Reliable Structure Generation Network (RSGNet see Section III-C) to generate the Speed Invariant Frame (SIF). Then the RGB image and SIF are respectively input into two independent CSPDarkNets to extract modality-specific features. The Adaptive Feature Completion Module (AFCM see Section III-D), which consists of an Event Refine Module (ERM) and a Lightness Distribution-aware Attention Module (LDAM) is inserted after the Conv and layer1 stages to perform the fusion of the two modalities. FPN+PANet fuses the features at different resolutions further. Finally, the decoder outputs each detected object’s class and bounding box information.

modalities for traffic object detection in variable illumination conditions. As depicted in Fig. 3(a), the SFNet takes both an RGB image and the corresponding event stream as input. First, a novel Reliable Structure Generation Network (RSGNet) is designed to generate a Speed Invariant Frame (SIF) from the event stream, containing complete structures and sharp edges. Subsequently, the RGB image and SIF are separately transferred to two independent feature extractors to extract modality-specific features. In this paper, we empirically choose CSPDarkNet [39] as the feature extractor. Further, to address information loss caused by non-uniform lighting, we propose an Adaptive Feature Completion Module (AFCM) to enable explicit interaction between the two modalities. As shown in Fig. 3(b-d), the AFCM comprises an Event Refine Module (ERM) that refines event features to suppress the influence of noise and a Lightness Distribution-aware Attention Module (LDAM) that adaptively fuses the event features into the RGB modality, enabling the modeling of illumination-robust feature representations. After that, the features with corresponding

resolutions of the two modalities are added and fed into FPN+PANet [40] [41] for further fusion. Finally, the fused features are fed into YOLOv5 [42] decoder to output class and bounding box information for each detected object.

### C. Reliable Structure Generation Network (RSGNet)

To achieve the fusion of images and events within a unified architecture, we opt to transform events into image-like tensors. Current image-like event representation methods often employ fixed time windows tailored to certain tasks and scenarios, resulting in sparse or blurry structural information for objects with varying speeds, which diminishes the expressiveness of the extracted features. To address this issue, we propose the RSGNet, which generates SIF with complete structures and sharp edges to accommodate diverse motion.

It’s important to note that the event output rate is directly proportional to the speed of motion and faster motion will output more events. Therefore, to guarantee information and structural integrity for all objects with varying speeds, we

adopt a large time window for sampling. In this paper, we choose Timestamp [16] to transfer event streams into frame  $F \in \mathbb{R}^{2 \times H \times W}$ . Timestamp partially retains time information while additionally capturing more details about slow-moving objects. Given the event stream  $\{(x_k, y_k, t_k, p_k)\}_{k=1}^N$  within the time window  $[0, T]$ .  $T$  is the time window duration which is set to 100 ms, and  $N$  represents the number of events. The expression is as follows:

$$F_{x,y,p} = \frac{\max_{x,y,p} \{t_j\}_{j=1}^n}{t_N}, \quad (2)$$

where  $n$  is the number of events with polarity  $p$  at  $(x, y)$ . In this way, complete structural information is extracted from the event stream. However, adopting a large time window inevitably results in elongated trajectories for fast-moving objects, leading to blurry edges in  $F$ .

To generate sharp edges from  $F$ , the discretized event polarity integration  $E \in \mathbb{R}^{B \times H \times W}$  is used to assist the network.  $E$  is computed following [21], and  $B$  is the number of time slices, which is set to 10. The expression is as follows:

$$t_k^* = \frac{B-1}{t_N - t_1} (t_k - t_1), \quad (3)$$

$$E_{x,y,t} = \sum_k p_k \max(0, 1 - |t - t_k^*|). \quad (4)$$

This is based on the fact that the motion of objects can cause frequent brightness changes at the edges and trigger enormous events. Therefore, through the discretization of time and the accumulation of event polarities in each time slice, the discretized event polarity integration can reveal the continuous motion information at the edges of objects and expose their motion patterns, which can guide the sharp edges generation from  $F$ .

Finally, the  $F$  and  $E$  are concatenated and fed into an encoder-decoder network to generate the SIF. The learning process can be formulated as:

$$SIF = M(F, E; \theta; S), \quad (5)$$

where  $M$  is the backbone of RSGNet, with U-Net [43] serving as  $M$  for this paper.  $\theta$  represents the learned parameters of  $M$ . The supervision signal  $S$  is represented by the edge maps extracted from the RGB images using the Sobel operator, which offers simple processing and noise robustness.

In this paper, we utilize the local cross-correlation loss function to assess the sharpness of SIF. This loss function, compared to L1 and L2, possesses greater robustness in handling information disparities between event data and RGB. Thus it is particularly well-suited for measuring alignment between two distributions in non-aligned conditions. The formula for this loss is as follows:

$$CC(SIF, S) = \sum_i \frac{\left( \sum_{q \in \Omega_i} (SIF(q) - \widehat{SIF}(i)) (S(q) - \hat{S}(i)) \right)^2}{\left( \sum_{q \in \Omega_i} (SIF(q) - \widehat{SIF}(i))^2 \right) \left( \sum_{q \in \Omega_i} (S(q) - \hat{S}(i))^2 \right)}, \quad (6)$$

$$\phi_{CC}(SIF) = -CC(SIF, S), \quad (7)$$

where  $\Omega$  is the local window size,  $\widehat{SIF}(i)$  and  $\hat{S}(i)$  represent the local mean around the pixel  $i$  in SIF and  $S$ , respectively.

In addition, we use TV loss to increase the contrast of SIF with the following equation:

$$\phi_{TV}(SIF) = -((\nabla_x SIF)^2 + (\nabla_y SIF)^2), \quad (8)$$

where  $\nabla_x$  and  $\nabla_y$  represent the horizontal and vertical gradient operations, respectively.

In summary, the total loss function of the RSGNet is:

$$\phi_{loss} = \phi_{CC}(SIF) + \phi_{TV}(SIF). \quad (9)$$

In this paper, we select 4,933 images with normal lighting from the DSEC dataset as the training set of RSGNet. After training, we fixed the RSGNet parameters and trained the SFNet backend. The inherent high dynamic range nature of event cameras enables the generalization of our RSGNet to different lighting conditions.

#### D. Adaptive Feature Completion Module (AFCM)

In variable illumination traffic scenes, the structural properties of poorly exposed images are disrupted, and information loss occurs. Due to the influence of non-uniform lighting, the degree of information loss across images is non-uniform. To adaptively compensate for the non-uniform information loss, we propose an AFCM, which consists of an ERM to refine the event features and a LDAM to adaptively fuse features from the event modality into the RGB modality, modeling illumination-robust feature representations.

Considering that event cameras inevitably generate noise due to their sensitivity to junction leakage current and photocurrent, and the event noise will result in errors and uncertainties in the generated representations, especially in low-light scenarios [22] [44]. We design an ERM that leverages the local smoothness of the RGB features  $f_R \in \mathbb{R}^{C \times H \times W}$  to eliminate the influence caused by event noise and refine the event features  $f_E \in \mathbb{R}^{C \times H \times W}$ . Specifically, a max pooling layer is applied along the channel dimension of  $f_R$  to extract distinctive features. To suppress the noise in improperly exposed conditions, an average pooling layer is employed along the channel dimension to smooth the extracted information. Subsequently, the feature maps obtained from the max pooling and average pooling steps are concatenated and further processed to generate a smooth mask map. This map exhibits lower response values in the smooth areas of the RGB features, effectively suppressing noise caused by junction leakage current and photocurrent in the event modality. The formula for the ERM is as follows:

$$\widetilde{f}_E = f_E \otimes \sigma(\text{Conv}(\text{Concat}(\text{APool}(f_R); \text{MPool}(f_R)))), \quad (10)$$

where APool is an average pooling layer, MPool is a max pooling layer, Concat indicates concatenation, Conv is a  $7 \times 7$  convolution layer,  $\sigma$  is sigmoid function,  $\otimes$  indicates element-wise multiplication, and  $\widetilde{f}_E$  is the refined event features.

Then, to achieve the adaptive fusion of the two modalities. We design a LDAM that computes the global spatial correlation  $GSC$  between  $f_R$  and  $\widetilde{f}_E$  to perceive global lightness

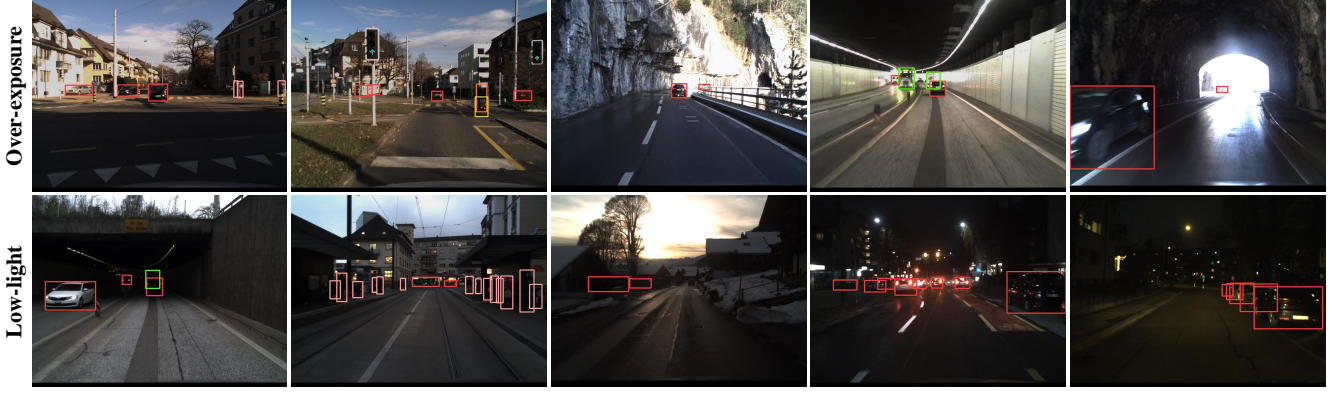


Fig. 4. Overview of our DSEC-Det dataset, which contains extremely challenging variable lighting conditions and rich object annotations.

distribution in  $f_R$ , and adaptively extracts event features to compensate information loss. The LDAM is defined as:

$$f'_R = \mathcal{T}(\text{Conv}_{1 \times 1}(f_R)), \quad (11)$$

$$\tilde{f}_{E1} = \mathcal{T}(\text{Conv}_{1 \times 1}(\tilde{f}_E)), \quad (12)$$

$$\tilde{f}_{E2} = \mathcal{T}(\text{Conv}_{1 \times 1}(\tilde{f}_E)), \quad (13)$$

$$GSC = \text{Softmax}(f'_R \cdot \tilde{f}_{E1}), \quad (14)$$

$$\tilde{f}'_E = \tilde{f}_{E2} \cdot GSC, \quad (15)$$

$$\tilde{f}_R = f_R + \text{Conv}_{1 \times 1}(\mathcal{T}(\tilde{f}'_E)), \quad (16)$$

where  $\mathcal{T}$  represents the matrix reshape operation and  $\cdot$  is matrix multiplication. The first three  $1 \times 1$  convolution layers are used to reduce the number of channels of  $f_R$  and  $\tilde{f}_E$ . The event features  $\tilde{f}_E$  required for RGB are generated through the multiplication of  $\tilde{f}_{E2}$  by the global spatial correlation map. Following a channel dimension recovery using an additional  $1 \times 1$  convolution,  $\tilde{f}'_E$  is combined with the original RGB features  $f_R$  to yield the finalized RGB features  $\tilde{f}_R$ .

#### IV. EXPERIMENTS

This section first describes the details of our proposed dataset. Then, we introduce the experimental settings. Subsequently, the quantitative and qualitative results are reported to demonstrate the effectiveness of our method. Finally, we conduct an ablation study on each module in our network.

##### A. DSEC-Det Dataset

Currently, some works [29] [30] propose RGB-Event object detection datasets based on the DSEC dataset [31]. Zhou *et al.* [30] selects 16 sequences from the DSEC dataset to introduce DSEC-MOD. However, this dataset is specifically designed for motion object detection tasks, solely providing labels for moving objects while omitting class information. Tomy *et al.* [29] uses pretrained YOLOv5 to generate object detection annotations. However, this dataset annotates only 41 DSEC sequences with three classes and contains a significant amount of noise.

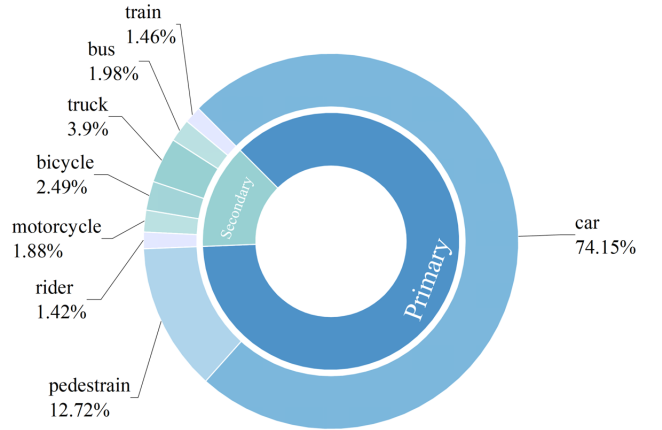


Fig. 5. Proportion of annotated bounding boxes for the DSEC-Det dataset.

Motivated by the scarcity of event-based datasets with high-quality and large-scale annotations, we construct a dataset using all 53 sequences from the DSEC dataset, which offers rich and accurate object annotations, as shown in Fig. 4. The DSEC dataset is a large RGB-Event dataset in autonomous driving scenarios, collected under extremely challenging variable lighting conditions. Such complex lighting conditions present a significant challenge for conventional cameras.

Specifically, we use homographic transformation based on camera matrices to align the viewpoint and resolution of the RGB and event cameras. Subsequently, we manually annotate all 53 sequences of the DSEC dataset, allocating 39 sequences for training and 14 for testing. For each sequence, we provide bounding box annotations for the following 8 classes, as shown in Fig. 5. The annotation file includes a list of labeled objects: each comprising the source image URL, the coordinates of the top-left of the bounding box, width, height and a class label. Considering the small resolution of  $640 \times 480$  of the event camera may impact the detection performance of small objects, we filter out bounding boxes with diagonals of less than 30 pixels following [13].

Table I presents a comparison between the DSEC-Det dataset and existing event-based datasets. Notably, the DSEC dataset was recently expanded by the original team [31],



TABLE I

COMPARISON OF DIFFERENT EVENT-BASED OBJECT DETECTION DATASETS IN DRIVING SCENARIOS. ‘‘AUTOMATED’’ REPRESENTS THE ANNOTATIONS GENERATED BY A PRETRAINED MODEL. ‘‘MANUAL’’ REPRESENTS THE ANNOTATIONS PRODUCED MANUALLY BY HUMAN ANNOTATORS, WHICH IS MORE ACCURATE.

Dataset	Intensity	Class	Resolution	Frames	Labeling method	Real	Public
Gen1 [32]	✗	2	304×240	16,984,800(39.32h)	Manual	✓	✓
1 Mpx [13]	✗	7	1280×720	3,164,400(14.65h)	Automated	✓	✓
EventKITTI [33]	RGB	8	1333×401	7,481	Manual	✗	✗
DSEC-MOD [30]	RGB	1	640×480	13,314	Manual	✓	✓
Tomy <i>et al.</i> [29]	RGB	3	640×480	44,776	Automated	✓	✓
DSEC-Detection [31]	RGB	8	640×480	70,379	Automated	✓	✓
Ours	RGB	8	640×480	63,931	Manual	✓	✓



Fig. 6. Comparison with Tomy *et al.* [29] and DSEC-Detection [31], whose annotations are generated by pretrained models. Both of them have cases of incorrect labels, especially in low-light conditions, and there is an offset between objects and bounding boxes in [29]. In contrast, our annotations produced manually by human annotators demonstrate higher accuracy and completeness. We utilize green and orange arrows to mark the missed and false detections.

incorporating additional sequences and utilizing a state-of-the-art object tracking algorithm for generating object detection annotations. However, the resulting labels also contain notable noise, as illustrated in Fig. 6. Such noise can significantly impact the model’s performance. In contrast, our annotations produced manually by human annotators are more accurate and comprehensive.

### B. Experimental Settings

**Datasets.** We evaluate the effectiveness of the SFNet on our proposed dataset DSEC-Det. In addition, to fairly compare with the state-of-the-art method RENet [30] that provides only their preprocessed results for the event modality without disclosing the processing code, we extract a subset from DSEC-Det called DSEC-Det-sub, consisting of sequences identical to those in DSEC-MOD.

From Fig. 5, we can observe the long tail properties, which present significant challenges. To evaluate the performance of our method under class-balanced and class-imbalanced

conditions, we partition the dataset into two versions. The first version contains the primary classes, consisting of car and pedestrian, with a relatively balanced number between them. The second version contains all classes, with a significant class imbalance issue.

**Implementation Details.** We utilize Adam optimizer with a learning rate of  $1e-4$  and a batch size of 8 to train the RSGNet. Subsequently, the weights of the RSGNet are kept fixed, and the SFNet is trained using Adam optimizer with a learning rate of  $1e-3$  and a batch size of 8.

**Evaluation Metrics.** We adopt COCO metrics [49] to evaluate the performance scores, including mAP50 with an IOU threshold of 50% and mAP50:95, which averages over IOUs between 50% and 95%.

### C. Quantitative results

To evaluate the superiority of our method, we compare our SFNet with SOTA (state-of-the-art) object detection methods, including frame-based methods and RGB-Event fusion-based

TABLE II  
PERFORMANCE COMPARISON WITH SOTA METHODS. THE BEST PERFORMANCE IS MARKED IN **BOLD**.

Model Type	Method	Event Representation	DSEC-Det				DSEC-Det-sub				
			Class-balanced		Class-imbalanced		Class-balanced		Class-imbalanced		
			mAP50	mAP50:95	mAP50	mAP50:95	mAP50	mAP50:95	mAP50	mAP50:95	
RGB	Faster-RCNN [45]	-	63.7	34.4	35.4	18.2	58.3	31.6	31.3	15.8	
	RetinaNet [46]	-	59.6	31.4	30.5	16.6	48.0	24.7	25.4	13.7	
	CenterNet [47]	-	63.6	19.1	35.1	10.4	56.7	17.8	30.3	9.5	
	YOLOv7-E6E [48]	-	62.3	37.8	31.5	18.2	50.1	27.0	23.4	12.5	
	YOLOv5-L(baseline) [42]	-	60.5	40.9	33.2	20.9	51.5	33.2	25.8	14.6	
RGB-Event	RENet [30]	E-TMA [30]	-	-	-	-	40.9	13.1	26.7	8.9	
	FPN-fusion [29]	Voxel [21]	59.3	32.2	28.9	15.2	48.8	23.5	26.6	13.1	
	FPN-fusion [29]+AFCM	SIF	62.4	35.2	32.8	18.6	51.3	29.7	27.0	14.9	
		Timestamp [16]	60.3	39.2	36.4	21.7	57.0	35.4	32.1	18.9	
		Time Surface [17]	61.6	39.3	39.5	25.2	57.6	36.2	30.8	19.5	
		DiST [19]	63.2	40.3	39.0	24.6	57.5	35.7	31.7	20.8	
		Voxel [21]	64.4	41.4	38.0	24.3	58.1	36.4	29.6	18.1	
		SFNet	SIF	<b>64.6</b>	<b>42.1</b>	<b>41.2</b>	<b>26.8</b>	<b>60.7</b>	<b>37.7</b>	<b>33.9</b>	<b>20.9</b>

methods. Moreover, to demonstrate the effectiveness and generality of our event representation method, we conduct comparative experiments with SOTA event representation methods.

**Comparison with SOTA object detection methods.** We compare our method with five frame-based methods: Faster-RCNN [45], RetinaNet [46], CenterNet [47], YOLOv5-L [42] and YOLOv7-E6E [48], as well as two SOTA RGB-Event object detection methods: FPN-fusion [29] and RENet [30]. The results are shown in Table II, SFNet<sup>†</sup> refers to the replacement of SIF with other event representation methods within the SFNet architecture. Our SFNet achieves better performance than the frame-based methods and significantly outperforms the existing two RGB-Event methods in both class-balanced and class-imbalanced situations. For example, our method outperforms the RGB baseline YOLOv5-L by 5.9% and FPN-fusion by 11.6% in mAP50:95 on the class-imbalanced situation of the DSEC-Det dataset. Notably, despite the inclusion of the event modality, both FPN-fusion and RENet exhibit lower performance than frame-based methods. In contrast, our method achieves more robust object detection in variable illumination conditions through motion-robust event representation and illumination-robust representations modeling based on effective cross-modality fusion. Moreover, replacing Voxel with our SIF and integrating our AFCM notably enhanced the performance of FPN-fusion. This improvement serves as evidence of the generalizability of our proposed modules.

**Comparison with SOTA event representation methods.** We compare our SIF with four SOTA event representation methods: Timestamp [16], Time Surface [17], DiST [19] and Voxel [21]. We keep the detection network and fusion module the same and only change the event representation method to demonstrate the effectiveness of our proposed SIF. As shown in the last five rows of Table II, our SIF, which contains the complete structures and sharp edges outperforms other event representation methods, yielding the best performance.

#### D. Qualitative results

**Comparison with the RGB baseline.** The detection results of our method and the RGB baseline YOLOv5-L under different lighting conditions are presented in Fig. 7. The first row shows a normal light scene, our method successfully detects the heavily occluded object with the help of contour information provided by our SIF. The second row exhibits an overexposed scene, and the subsequent three rows show low-light scenes. By effectively leveraging the complementary nature of the two modalities and modeling illumination-robust feature representations, our method exhibits superior robustness compared to the RGB baseline in complex lighting scenes, enabling the successful detection of a greater number of objects.

**Comparison with SOTA event representation methods.** The detection results of our method compared to Voxel [21], Timestamp [16], Time Surface [17], and DiST [19] are shown in Fig. 8. The first two rows depict scenes with slowly moving objects, and the last row shows a scene with fast-moving objects. In the first row, the black car on the left exhibits a limited number of triggered events due to its slow motion relative to the camera and blending with the dark background. Other event representation methods produce sparse contours that are prone to blending with background noise, resulting in detection failures. In the last row, other methods produce blurry structures for the rider that disrupt the structural information, resulting in detection failures. In contrast, our RSGNet can generate complete structures and sharp edges in the SIF, enabling successful detection. Additionally, the comparison also shows a slight denoising effect in the SIF, owing to the local smoothness of RGB images.

#### E. Ablation Study

In this section, we present the ablation study results to demonstrate the effectiveness of each part of our SFNet.





Fig. 7. Qualitative comparison with RGB baseline on the class-imbalanced situation of the DSEC-Det dataset. We utilize **green** arrows to mark the failed cases.

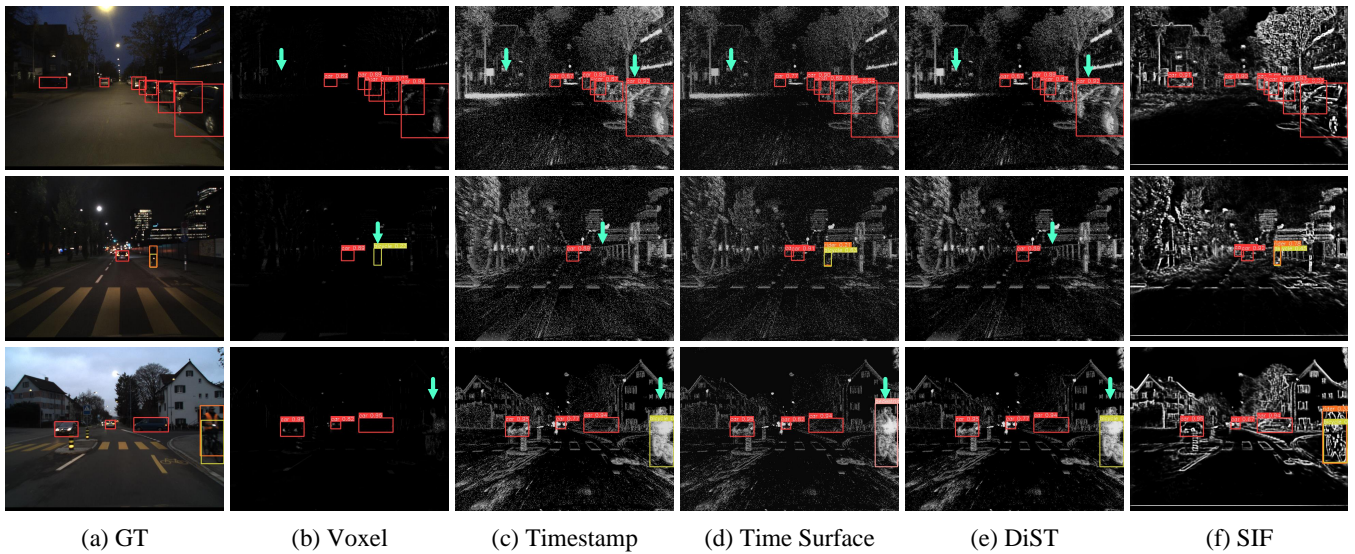


Fig. 8. Qualitative comparison with SOTA event representation methods on the class-imbalanced situation of the DSEC-Det dataset. We utilize **green** arrows to mark the failed cases.

TABLE III  
THE PERFORMANCE OF OUR COMPONENTS. THE **RED BOLD** AND **BLUE BOLD** REPRESENT THE IMPROVEMENT AND SLIGHT DEGRADATION COMPARED TO THE BASELINE. THE BEST PERFORMANCE IS MARKED IN **BLACK BOLD**.

SIF	ERM	LDAM	DSEC-Det				DSEC-Det-sub			
			Class-balanced		Class-imbalanced		Class-balanced		Class-imbalanced	
			mAP50	mAP50:95	mAP50	mAP50:95	mAP50	mAP50:95	mAP50	mAP50:95
			60.5	40.9	33.2	20.9	51.5	33.2	25.8	14.6
✓			<b>62.3+1.8</b>	<b>40.8-0.1</b>	<b>36.8+3.6</b>	<b>24.2+3.3</b>	<b>56.6+5.1</b>	<b>37.0+3.8</b>	<b>30.6+4.8</b>	<b>19.2+4.6</b>
✓	✓		<b>61.8+1.3</b>	<b>40.3-0.6</b>	<b>35.0+1.8</b>	<b>23.3+2.4</b>	<b>55.2+3.7</b>	<b>36.0+2.8</b>	<b>30.7+4.9</b>	<b>18.5+3.9</b>
✓		✓	<b>63.8+3.3</b>	<b>41.8+0.9</b>	<b>35.2+2.0</b>	<b>22.2+1.3</b>	<b>59.0+7.5</b>	<b>36.8+3.6</b>	<b>33.0+7.2</b>	<b>19.4+4.8</b>
✓	✓	✓	<b>64.6+4.1</b>	<b>42.1+1.2</b>	<b>41.2+8.0</b>	<b>26.8+5.9</b>	<b>60.7+9.2</b>	<b>37.7+4.5</b>	<b>33.9+8.1</b>	<b>20.9+6.3</b>

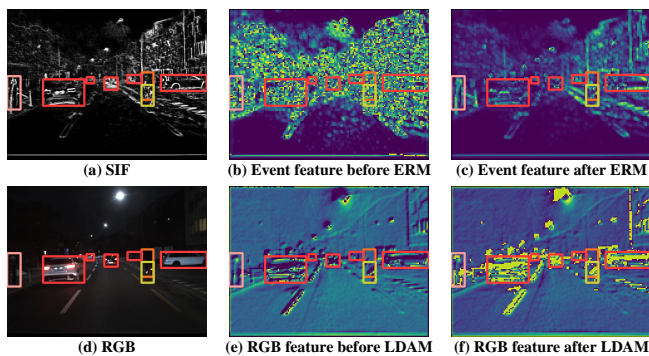


Fig. 9. Feature maps of RGB and event modalities before and after AFCM.

**Contribution of our SFNet components.** We take YOLOv5-L [42] as the RGB baseline to perform a comprehensive ablation study and analyze the performance of each component in the SFNet. Table III shows the results from different combinations of modules in our method. We can observe that the model achieves higher performance with the help of the SIF. Combined with the AFCM, which consists of an ERM and a LDAM, our whole network significantly outperforms the baseline, validating the effectiveness of each proposed module under variable illumination traffic scenes. Although the ERM results in a slight decrease in performance, its integration with the LDAM can yield improved overall performance. This synergy is attributed to the ERM’s ability to filter out extraneous information, enabling the LDAM to extract more valuable features from the event modality.

The feature maps before and after applying the AFCM are visualized in Fig. 9, and the visualizations illustrate the effects of the ERM and LDAM. In Fig. 9(b, c), the ERM guides the event modality to re-integrate with the background and suppress noise. In Fig. 9(e, f), the LDAM perceives regions of information loss caused by non-uniform lighting in the RGB modality and performs adaptive completion.

**Duration of the time window  $T$ .** To investigate the impact of different time window durations on detection performance, we conduct experiments comparing performance using various time windows. We use time windows of 50 ms, 100 ms, and 150 ms, corresponding to one, two, and three times the inter-frame interval of the image, respectively. As presented in Table IV, the 100 ms time window delivers optimal performance,

TABLE IV  
THE PERFORMANCE OF DIFFERENT TIME WINDOW. THE BEST PERFORMANCE IS MARKED IN **BOLD**.

$T$	DSEC-Det				DSEC-Det-sub			
	Class-balanced		Class-imbalanced		Class-balanced		Class-imbalanced	
	mAP50	mAP50:95	mAP50	mAP50:95	mAP50	mAP50:95	mAP50	mAP50:95
50 ms	64.0	42.0	36.3	23.1	57.9	35.3	33.4	19.8
100 ms	<b>64.6</b>	<b>42.1</b>	<b>41.2</b>	<b>26.8</b>	<b>60.7</b>	<b>37.7</b>	<b>33.9</b>	<b>20.9</b>
150 ms	64.1	41.0	36.7	23.5	58.2	35.7	34.1	20.2

TABLE V  
THE PERFORMANCE OF DIFFERENT SUPERVISION SIGNALS. THE BEST PERFORMANCE IS MARKED IN **BOLD**.

$S$	DSEC-Det				DSEC-Det-sub			
	Class-balanced		Class-imbalanced		Class-balanced		Class-imbalanced	
	mAP50	mAP50:95	mAP50	mAP50:95	mAP50	mAP50:95	mAP50	mAP50:95
Sobel	<b>64.6</b>	<b>42.1</b>	<b>41.2</b>	<b>26.8</b>	<b>60.7</b>	<b>37.7</b>	<b>33.9</b>	<b>20.9</b>
Roberts	60.7	40.4	36.6	23.8	54.1	33.4	29.7	17.9
Laplace	62.9	41.1	39.6	25.6	57.9	35.3	32.9	18.9

achieving a harmonious balance between information content and recovery complexity. In contrast, the 50 ms time window, being brief, lacks sufficient data, making it challenging to extract complete structural details. The 150 ms time window, although rich in information, suffers from excessive duration, resulting in overly prolonged motion trajectories within the scene, consequently impeding the recovery of sharp structures.

**Selection of the supervision signal  $S$ .** To assess the impact of different supervision signals on final detection performance, we conduct experimental comparisons of object detection results using the first-order differential operators Sobel and Roberts, as well as the second-order differential operator Laplace. The results present in Table V clearly demonstrate the significant superiority of the Sobel operator over the Roberts and Laplace operators. This difference in performance can be attributed to the incompleteness of edge information extracted by the Roberts operator in the diagonal direction, which in turn affects the recovery of sharp edges in SIF. Additionally, the Laplace operator, as a second-order differential operator, exhibits sensitivity to noise, exacerbating its impact. In contrast, the Sobel operator excels at extracting more comprehensive edges while maintaining robustness in the presence of noise.

**Contribution of the loss functions in the RSGNet.** We

TABLE VI  
THE PERFORMANCE OF OUR LOSS FUNCTIONS. THE BEST PERFORMANCE IS MARKED IN **BOLD**.

$\phi_{CC}$	$\phi_{TV}$	DSEC-Det				DSEC-Det-sub			
		Class-balanced		Class-imbalanced		Class-balanced		Class-imbalanced	
		mAP50	mAP50:95	mAP50	mAP50:95	mAP50	mAP50:95	mAP50	mAP50:95
✓		64.4	42.1	38.8	25.2	57.2	36.1	30.8	19.8
✓	✓	<b>64.6</b>	<b>42.1</b>	<b>41.2</b>	<b>26.8</b>	<b>60.7</b>	<b>37.7</b>	<b>33.9</b>	<b>20.9</b>

TABLE VII  
THE PERFORMANCE OF OUR MODEL WITH AFCM PLACED AFTER DIFFERENT LAYERS. THE BEST PERFORMANCE IS MARKED IN **BOLD**.

Conv	layer1	layer2	layer3	layer4	DSEC-Det				DSEC-Det-sub			
					Class-balanced		Class-imbalanced		Class-balanced		Class-imbalanced	
					mAP50	mAP50:95	mAP50	mAP50:95	mAP50	mAP50:95	mAP50	mAP50:95
					62.3	40.8	36.8	24.2	56.6	37.0	30.6	19.2
✓					63.0	41.4	38.8	24.9	58.4	35.6	31.2	19.8
✓	✓				<b>64.6</b>	42.1	<b>41.2</b>	<b>26.8</b>	<b>60.7</b>	<b>37.7</b>	33.9	20.9
✓	✓	✓			63.8	41.9	36.3	22.4	58.9	35.4	<b>35.7</b>	20.9
✓	✓	✓	✓		<b>64.6</b>	<b>42.4</b>	35.8	22.2	58.2	35.1	35.3	<b>21.3</b>
✓	✓	✓	✓	✓	63.5	41.5	37.7	23.2	56.6	34.1	29.1	19.0

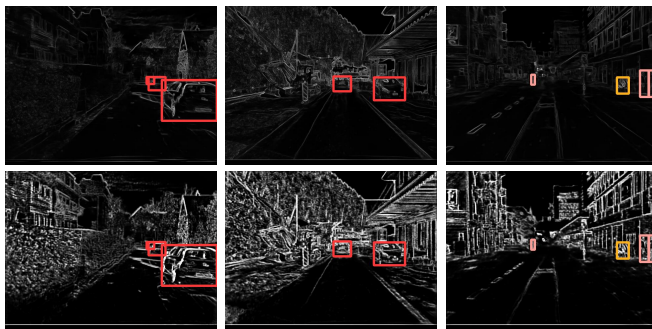


Fig. 10. The results of RSGNet trained with different loss functions. The first row corresponds to SIF with  $\phi_{CC}$ , while the second row corresponds to SIF with both  $\phi_{CC}$  and  $\phi_{TV}$ .

next conduct an ablation study to analyze the contribution of the loss functions of our RSGNet. The results in Table VI demonstrate that the absence of TV loss leads to a performance decrease, indicating the significance of TV loss in achieving high accuracy. Moreover, Fig. 10 visually depicts the effect of adding the TV loss, showcasing a substantial enhancement in the contrast of the SIF and the clarity of edges.

**AFCM placement.** Finally, we conduct an ablation study to analyze the relationship between detection performance and the AFCM placement. Table VII illustrates that placing the AFCM after the Conv and layer1 obtains the largest improvement compared with other placements. Naturally, the results agree with our motivation that completing the low-level features such as structural features adaptively in the RGB modality is beneficial.

## V. CONCLUSION

In this paper, we propose a novel RGB-Event fusion architecture SFNet for traffic object detection in challenging

illumination conditions, which consists of two key components: a RSGNet and an AFCM. The RSGNet can generate SIF with complete structures and sharp edges from the event stream to accommodate diverse motion. Additionally, the AFCM can achieve adaptive fusion of the two modalities to address information loss caused by non-uniform lighting. Furthermore, we propose a large-scale DSEC-Det dataset for traffic object detection with rich and accurate annotations. The experimental results demonstrate that our method outperforms SOTA methods and boosts the robustness of traffic object detection in variable illumination conditions by leveraging the complementarities of the two modalities effectively. We focus on developing a multi-modal fusion framework to enhance the robustness of object detection in varying lighting conditions. We have yet to fully exploit the spatial sparsity and high temporal resolution of event cameras. Therefore, in the future, we will concentrate on the following two aspects: 1) We will explore a novel fusion framework that can achieve low-latency and high-frame-rate object detection by leveraging the spatial sparsity and high temporal resolution of event cameras. 2) We will construct a highly annotated RGB-Event dataset for intelligent transportation systems to further advance this field.

## REFERENCES

- [1] H. Zhang, G. Luo, J. Li, and F.-Y. Wang, "C2fda: Coarse-to-fine domain adaptation for traffic object detection," *IEEE Transactions on Intelligent Transportation Systems*, vol. 23, no. 8, pp. 12 633–12 647, 2021.
- [2] R. O. Chavez-Garcia and O. Aycard, "Multiple sensor fusion and classification for moving object detection and tracking," *IEEE Transactions on Intelligent Transportation Systems*, vol. 17, no. 2, pp. 525–534, 2015.
- [3] M. Shirpour, N. Khairdoost, M. Bauer, and S. Beauchemin, "Traffic object detection and recognition based on the attentional visual field of drivers," *IEEE Transactions on Intelligent Vehicles*, 2021.
- [4] H. Ghahremanzhad, H. Shi, and C. Liu, "Object detection in traffic videos: A survey," *IEEE Transactions on Intelligent Transportation Systems*, 2023.

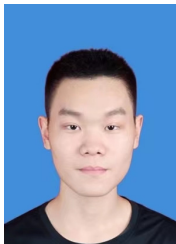


- [5] P. Lichtsteiner, C. Posch, and T. Delbruck, "A  $128 \times 128$  120 db 15  $\mu$ s latency asynchronous temporal contrast vision sensor," *IEEE Journal of Solid-State Circuits*, vol. 43, no. 2, pp. 566–576, 2008.
- [6] C. Posch, D. Matolin, and R. Wohlgenannt, "A qvga 143 db dynamic range frame-free pwm image sensor with lossless pixel-level video compression and time-domain cds," *IEEE Journal of Solid-State Circuits*, vol. 46, no. 1, pp. 259–275, 2011.
- [7] C. Brandli, R. Berner, M. Yang, S.-C. Liu, and T. Delbruck, "A  $240 \times 180$  130 db 3  $\mu$ s latency global shutter spatiotemporal vision sensor," *IEEE Journal of Solid-State Circuits*, vol. 49, no. 10, pp. 2333–2341, 2014.
- [8] V. Brebion, J. Moreau, and F. Davoine, "Real-time optical flow for vehicular perception with low-and high-resolution event cameras," *IEEE Transactions on Intelligent Transportation Systems*, vol. 23, no. 9, pp. 15 066–15 078, 2021.
- [9] F. Munir, S. Azam, M. Jeon, B.-G. Lee, and W. Pedrycz, "Ldnet: End-to-end lane marking detection approach using a dynamic vision sensor," *IEEE Transactions on Intelligent Transportation Systems*, vol. 23, no. 7, pp. 9318–9334, 2021.
- [10] J. Chen, Y. Wang, Y. Cao, F. Wu, and Z.-J. Zha, "Progressivemotionseg: Mutually reinforced framework for event-based motion segmentation," in *Proceedings of the AAAI Conference on Artificial Intelligence*, vol. 36, no. 1, 2022, pp. 303–311.
- [11] G. Tan, Y. Wang, H. Han, Y. Cao, F. Wu, and Z.-J. Zha, "Multi-grained spatio-temporal features perceived network for event-based lip-reading," in *Proceedings of the IEEE/CVF Conference on Computer Vision and Pattern Recognition*, 2022, pp. 20 094–20 103.
- [12] Y. Li, J. Moreau, and J. Ibanez-Guzman, "Emergent visual sensors for autonomous vehicles," *IEEE Transactions on Intelligent Transportation Systems*, vol. 24, no. 5, pp. 4716–4737, 2023.
- [13] E. Perot, P. De Tournemire, D. Nitti, J. Masci, and A. Sironi, "Learning to detect objects with a 1 megapixel event camera," *Advances in Neural Information Processing Systems*, vol. 33, pp. 16 639–16 652, 2020.
- [14] A. I. Maqueda, A. Loquercio, G. Gallego, N. Garcia, and D. Scaramuzza, "Event-based vision meets deep learning on steering prediction for self-driving cars," in *Proceedings of the IEEE conference on computer vision and pattern recognition*, 2018, pp. 5419–5427.
- [15] A. Z. Zhu, L. Yuan, K. Chaney, and K. Daniilidis, "Ev-flownet: Self-supervised optical flow estimation for event-based cameras," *arXiv preprint arXiv:1802.06898*, 2018.
- [16] P. K. Park, B. H. Cho, J. M. Park, K. Lee, H. Y. Kim, H. A. Kang, H. G. Lee, J. Woo, Y. Roh, W. J. Lee *et al.*, "Performance improvement of deep learning based gesture recognition using spatiotemporal demosaicing technique," in *2016 IEEE International Conference on Image Processing (ICIP)*. IEEE, 2016, pp. 1624–1628.
- [17] X. Lagorce, G. Orchard, F. Galluppi, B. E. Shi, and R. B. Benosman, "Hots: a hierarchy of event-based time-surfaces for pattern recognition," *IEEE transactions on pattern analysis and machine intelligence*, vol. 39, no. 7, pp. 1346–1359, 2016.
- [18] A. Sironi, M. Brambilla, N. Bourdis, X. Lagorce, and R. Benosman, "Hats: Histograms of averaged time surfaces for robust event-based object classification," in *Proceedings of the IEEE conference on computer vision and pattern recognition*, 2018, pp. 1731–1740.
- [19] J. Kim, J. Bae, G. Park, D. Zhang, and Y. M. Kim, "N-imagenet: Towards robust, fine-grained object recognition with event cameras," in *Proceedings of the IEEE/CVF International Conference on Computer Vision*, 2021, pp. 2146–2156.
- [20] A. Zihao Zhu, L. Yuan, K. Chaney, and K. Daniilidis, "Unsupervised event-based optical flow using motion compensation," in *Proceedings of the European Conference on Computer Vision (ECCV) Workshops*, 2018, pp. 0–0.
- [21] A. Z. Zhu, L. Yuan, K. Chaney, and K. Daniilidis, "Unsupervised event-based learning of optical flow, depth, and egomotion," in *Proceedings of the IEEE/CVF Conference on Computer Vision and Pattern Recognition*, 2019, pp. 989–997.
- [22] Z. Wan, Y. Wang, G. Tan, Y. Cao, and Z.-J. Zha, "S2n: Suppression-strengthen network for event-based recognition under variant illuminations," in *Computer Vision–ECCV 2022: 17th European Conference, Tel Aviv, Israel, October 23–27, 2022, Proceedings, Part III*. Springer, 2022, pp. 716–733.
- [23] K. Sun, W. Wu, T. Liu, S. Yang, Q. Wang, Q. Zhou, Z. Ye, and C. Qian, "Fab: A robust facial landmark detection framework for motion-blurred videos," in *Proceedings of the IEEE/CVF International Conference on Computer Vision*, 2019, pp. 5462–5471.
- [24] N. F. Chen, "Pseudo-labels for supervised learning on dynamic vision sensor data, applied to object detection under ego-motion," in *Proceedings of the IEEE conference on computer vision and pattern recognition workshops*, 2018, pp. 644–653.
- [25] Z. Jiang, P. Xia, K. Huang, W. Stechele, G. Chen, Z. Bing, and A. Knoll, "Mixed frame-/event-driven fast pedestrian detection," in *2019 International Conference on Robotics and Automation (ICRA)*. IEEE, 2019, pp. 8332–8338.
- [26] J. Li, S. Dong, Z. Yu, Y. Tian, and T. Huang, "Event-based vision enhanced: A joint detection framework in autonomous driving," in *2019 IEEE international conference on multimedia and expo (icme)*. IEEE, 2019, pp. 1396–1401.
- [27] M. Liu, N. Qi, Y. Shi, and B. Yin, "An attention fusion network for event-based vehicle object detection," in *2021 IEEE International Conference on Image Processing (ICIP)*. IEEE, 2021, pp. 3363–3367.
- [28] H. Cao, G. Chen, J. Xia, G. Zhuang, and A. Knoll, "Fusion-based feature attention gate component for vehicle detection based on event camera," *IEEE Sensors Journal*, vol. 21, no. 21, pp. 24 540–24 548, 2021.
- [29] A. Tomy, A. Paigwar, K. S. Mann, A. Renzaglia, and C. Laugier, "Fusing event-based and rgb camera for robust object detection in adverse conditions," in *2022 International Conference on Robotics and Automation (ICRA)*. IEEE, 2022, pp. 933–939.
- [30] Z. Zhou, Z. Wu, R. Boutheau, F. Yang, C. Demonceaux, and D. Ginjac, "Rgb-event fusion for moving object detection in autonomous driving," *arXiv preprint arXiv:2209.08323*, 2022.
- [31] M. Gehrig, W. Aarents, D. Gehrig, and D. Scaramuzza, "Dsec: A stereo event camera dataset for driving scenarios," *IEEE Robotics and Automation Letters*, vol. 6, no. 3, pp. 4947–4954, 2021.
- [32] P. De Tournemire, D. Nitti, E. Perot, D. Migliore, and A. Sironi, "A large scale event-based detection dataset for automotive," *arXiv preprint arXiv:2001.08499*, 2020.
- [33] Z. Liang, H. Cao, C. Yang, Z. Zhang, and G. Chen, "Global-local feature aggregation for event-based object detection on eventkitti," in *2022 IEEE International Conference on Multisensor Fusion and Integration for Intelligent Systems (MFI)*. IEEE, 2022, pp. 1–7.
- [34] H. Rebecq, D. Gehrig, and D. Scaramuzza, "Esim: an open event camera simulator," in *Conference on robot learning*. PMLR, 2018, pp. 969–982.
- [35] A. Geiger, P. Lenz, and R. Urtasun, "Are we ready for autonomous driving? the kitti vision benchmark suite," in *2012 IEEE conference on computer vision and pattern recognition*. IEEE, 2012, pp. 3354–3361.
- [36] J. Li, J. Li, L. Zhu, X. Xiang, T. Huang, and Y. Tian, "Asynchronous spatio-temporal memory network for continuous event-based object detection," *IEEE Transactions on Image Processing*, vol. 31, pp. 2975–2987, 2022.
- [37] M. Gehrig and D. Scaramuzza, "Recurrent vision transformers for object detection with event cameras," in *Proceedings of the IEEE/CVF Conference on Computer Vision and Pattern Recognition*, 2023, pp. 13 884–13 893.
- [38] G. Gallego, T. Delbrück, G. Orchard, C. Bartolozzi, B. Taba, A. Censi, S. Leutenegger, A. J. Davison, J. Conrad, K. Daniilidis *et al.*, "Event-based vision: A survey," *IEEE transactions on pattern analysis and machine intelligence*, vol. 44, no. 1, pp. 154–180, 2020.
- [39] A. Bochkovskiy, C.-Y. Wang, and H.-Y. M. Liao, "Yolov4: Optimal speed and accuracy of object detection," *arXiv preprint arXiv:2004.10934*, 2020.
- [40] T.-Y. Lin, P. Dollár, R. Girshick, K. He, B. Hariharan, and S. Belongie, "Feature pyramid networks for object detection," in *Proceedings of the IEEE conference on computer vision and pattern recognition*, 2017, pp. 2117–2125.
- [41] S. Liu, L. Qi, H. Qin, J. Shi, and J. Jia, "Path aggregation network for instance segmentation," in *Proceedings of the IEEE conference on computer vision and pattern recognition*, 2018, pp. 8759–8768.
- [42] G. Jocher, "YOLOv5 by Ultralytics," May 2020. [Online]. Available: <https://github.com/ultralytics/yolov5>
- [43] O. Ronneberger, P. Fischer, and T. Brox, "U-net: Convolutional networks for biomedical image segmentation," in *Medical Image Computing and Computer-Assisted Intervention–MICCAI 2015: 18th International Conference, Munich, Germany, October 5–9, 2015, Proceedings, Part III 18*. Springer, 2015, pp. 234–241.
- [44] S. Ding, J. Chen, Y. Wang, Y. Kang, W. Song, J. Cheng, and Y. Cao, "E-mlb: Multilevel benchmark for event-based camera denoising," *IEEE Transactions on Multimedia*, 2023.
- [45] S. Ren, K. He, R. Girshick, and J. Sun, "Faster r-cnn: Towards real-time object detection with region proposal networks," *Advances in neural information processing systems*, vol. 28, 2015.
- [46] T.-Y. Lin, P. Goyal, R. Girshick, K. He, and P. Dollár, "Focal loss for dense object detection," in *Proceedings of the IEEE international conference on computer vision*, 2017, pp. 2980–2988.

- [47] X. Zhou, D. Wang, and P. Krähenbühl, "Objects as points," *arXiv preprint arXiv:1904.07850*, 2019.
- [48] C.-Y. Wang, A. Bochkovskiy, and H.-Y. M. Liao, "Yolov7: Trainable bag-of-freebies sets new state-of-the-art for real-time object detectors," in *Proceedings of the IEEE/CVF Conference on Computer Vision and Pattern Recognition*, 2023, pp. 7464–7475.
- [49] T.-Y. Lin, M. Maire, S. Belongie, J. Hays, P. Perona, D. Ramanan, P. Dollár, and C. L. Zitnick, "Microsoft coco: Common objects in context," in *Computer Vision—ECCV 2014: 13th European Conference, Zurich, Switzerland, September 6–12, 2014, Proceedings, Part V 13*. Springer, 2014, pp. 740–755.



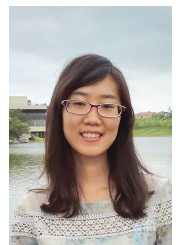
**Zhanwen Liu** (Member, IEEE) received the B.S. degree from Northwestern Polytechnical University, Xi'an, China, in 2006, the M.S. and the Ph.D. degrees in Traffic Information Engineering and Control from Chang'an University, Xi'an, China, in 2009 and 2014 respectively. She is currently a professor with School of Information Engineering, Chang'an University, Xi'an, China. Her research interests include vision perception, autonomous vehicles, deep learning and intelligent transportation systems.



**Nan Yang** received the B.S. degree from Chang'an University in Xi'an, China, in 2022, where he is currently working toward the Ph.D. degree in Traffic Information Engineering and Control. His current research interests include object detection and multiple-object tracking based on event cameras, and their applications in intelligent vehicle and road infrastructure perception.



**Yang Wang** (Member, IEEE) received the B.S. degree from Chang'an University, Xi'an, China, in 2016, the Ph.D. degree in control science and engineering from the University of Science and Technology of China, in 2021. He is currently an Associate professor with the School of Information Engineering, Chang'an University, Xi'an, China. His central research interests focus on computer vision and multimedia processing.



**Yuke Li** received the B.E. degree in Communication Engineering from Xidian University, Xi'an, China, in 2014, the Ph.D. degree in Control Theory and Control Engineering at the State Key Laboratory of Management and Control for Complex Systems, Institute of Automation, Chinese Academy of Sciences, Beijing, China, in 2019. From November 2016 to November 2017, she was a Visiting Scholar with Colorado State University, Fort Collins, CO, USA. From October 2021 to October 2023, she was a Postdoctoral Researcher at Huawei Technologies

Co., Ltd. Now she is a Senior Engineer at Waytous Co. Ltd., Beijing, China. Her research interests include intelligent transportation systems, parallel intelligence, signal processing, and joint radar and communication. She received the Best Paper Award from the IEEE International Conference on Intelligent Transportation Systems in 2014, Beijing Outstanding Graduates Award in 2019, and Huawei Outstanding Postdoctoral Fellow in 2023.



**Xiangmo Zhao** (Member, IEEE) received the B.S. degree from Chongqing University, China, in 1987, and the M.S. and Ph.D. degrees from Chang'an University, China, in 2002 and 2005, respectively. He is currently a distinguished professor with School of Information Engineering, Chang'an University, Xi'an, China. His research interests include intelligent transportation systems, internet of vehicles, connected and autonomous vehicles testing technology.



**Fei-Yue Wang** (Fellow, IEEE) received the Ph.D. degree in computer and systems engineering from the Rensselaer Polytechnic Institute, Troy, NY, USA, in 1990.

He joined The University of Arizona in 1990 and became a Professor and the Director of the Robotics and Automation Laboratory and the Program in Advanced Research for Complex Systems. In 1999, he founded the Intelligent Control and Systems Engineering Center, Institute of Automation, Chinese Academy of Sciences (CAS), Beijing, China, under

the support of the Outstanding Chinese Talents Program from the State Planning Council. In 2002, he was appointed as the Director of the Key Laboratory for Complex Systems and Intelligence Science, CAS, where he was the Vice President of the Institute of Automation, in 2006. He found CAS Center for Social Computing and Parallel Management in 2008, and became the State Specially Appointed Expert and the Founding Director of the State Key Laboratory for Management and Control of Complex Systems in 2011. His current research focuses on methods and applications for parallel intelligence, social computing, DeSci, and knowledge automation.

He is a fellow of INCOSE, IFAC, ASME, and AAAS. In 2007, he received the National Prize in Natural Sciences of China and numerous best papers awards from IEEE TRANSACTIONS. He became an Outstanding Scientist of ACM for his work in intelligent control and social computing. He received the IEEE ITS Outstanding Application and Research Awards in 2009, 2011, and 2015; and the IEEE SMC Norbert Wiener Award in 2014. Since 1997, he has been serving as the general chair or the program chair for over 30 IEEE, INFORMS, IFAC, ACM, and ASME conferences. He was the President of the IEEE ITS Society, from 2005 to 2007; the IEEE Council of RFID, from 2019 to 2021; the Chinese Association for Science and Technology, USA, in 2005; the American Zhu Kezhen Education Foundation, from 2007 to 2008. He was the Vice President of the ACM China Council, from 2010 to 2011; and the IEEE Systems, Man, and Cybernetics Society, from 2019 to 2021. He was the Vice President and the Secretary General of the Chinese Association of Automation, from 2008 to 2018. He was the Founding Editor-in-Chief (EiC) of the International Journal of Intelligent Control and Systems, from 1995 to 2000; IEEE Intelligent Transportation Systems Magazine, from 2006 to 2007; IEEE/CAA JOURNAL OF AUTOMATICA SINICA, from 2014 to 2017; China's Journal of Command and Control, from 2015 to 2021; and China's Journal of Intelligent Science and Technology, from 2019 to 2021. He was the EiC of the IEEE INTELLIGENT SYSTEMS, from 2009 to 2012, IEEE TRANSACTIONS ON INTELLIGENT TRANSPORTATION SYSTEMS, from 2009 to 2016, and IEEE TRANSACTIONS ON COMPUTATIONAL SOCIAL SYSTEMS, from 2017 to 2020. Currently, he is the President of the CAA's Supervision Council, and the EiC of IEEE TRANSACTION ON INTELLIGENT VEHICLES. He became the IFAC Pavel J. Nowacki Distinguished Lecturer in 2021.